Comput Mech (2005) 36: 459–474
DOI 10.1007/s00466-005-0681-6

ORIGINAL PAPER

Z. Q. Yue · H. T. Xiao · L. G. Tham · C. F. Lee
E. Pan

Boundary element analysis of three-dimensional crack problems in two joined transversely isotropic solids

Received: 6 October 2004 / Accepted: 24 February 2005 / Published online: 14 April 2005

Abstract The present paper presents a boundary element analysis of penny-shaped crack problems in two joined transversely isotropic solids. The boundary element analysis is carried out by incorporating the fundamental singular solution for a concentrated point load in a transversely isotropic bi-material solid of infinite space into the conventional displacement boundary integral equations. The conventional multi-region method is used to analyze the crack problems. The traction-singular elements are employed to capture the singularity around the crack front. The values of the stress intensity factors are obtained by using crack opening displacements. The numerical scheme results are verified with the closed-form solutions available in the literature for a penny-shaped crack parallel to the plane of the isotropy of a homogeneous and transversely isotropic solid of infinite extent. The new problem of a penny-shaped crack perpendicular to the interface of a transversely isotropic bi-material solid is then examined in detail. The crack surfaces are subject to the three normal tractions and the uniform shear traction. The associated stress intensity factor values are obtained and analyzed. The present results can be used for the prediction of the stability of composite structures and the hydraulic fracturing in deep rock strata and reservoir engineering.

Z. Q. Yue (✉) · H. T. Xiao · L. G. Tham · C. F. Lee
Department of Civil Engineering, The University of Hong Kong, Pokfulam Road, Hong Kong, P.R. China
E-mail: yueqzq@hkucc.hku.hk
Tel.: +852-2859-1967
Fax: +852-2559-5337

E. Pan
Department of Civil Engineering, University of Akron, Akron, OH, 44325-3905 USA

Keywords Crack · Boundary element method · Fundamental singular solution · Anisotropy · Bi-materials · Stress intensity factors · Fracture mechanics

1 Introduction

It has been well recognized that geomaterials such as sedimentary rocks can be transversely isotropic in their material properties, because during their formation, they usually were subject to a dominant force action such as gravity along one specific direction. In recent years, many types of composite materials have been fabricated and used for structural components. Some of the man-made materials such as fiber reinforced plastics and unidirectionally solidified eutectic alloys can also have the properties to be isotropic along a series of parallel planes and anisotropic along the direction perpendicular to the isotropic planes. It is evident that these transversely isotropic materials can contain flaws or imperfections or cracks. It has always been an interesting and important task for scientists and engineers to quantify and predict the crack behavior of these anisotropic materials under external loading. Effort and achievements on this task before 1982 can be found in a review report by Mura (1982). In the ensuing, we shall give a brief review on the work and findings available in the open literature that are mostly relevant to crack problems in anisotropic materials.

Sih et al. (1965) published one of their classic findings about cracks in rectilinearly anisotropic bodies. They found that an elastic singularity of the order $r^{1/2}$ is always present at the crack front in a body with rectilinear anisotropy and the magnitude of the local stresses may be described in terms of stress intensity factors. Kassir and Sih (1975) and Sih and Chen (1981) further investigated a number of crack problems in anisotropic solids and composites. In particular, Kassir and Sih (1968), Hoeing (1978) and Zhang and Mai (1989) gave the exact

closed-form solutions for the modes I, II and III stress intensity factors (SIFs) associated with a penny-shaped or elliptical crack in a transversely isotropic elastic solid occupying infinite space, where the plane of the crack surface is parallel to the plane of the material isotropy. Hoenig (1978) further gave the SIFs, only in terms of compact line integral expressions, for a penny- shaped or elliptical crack in the infinite anisotropic solid, where the plane of the crack surface is not parallel to the plane of the material isotropy.

In the application of large-scale hydraulic fracturing, vertical cracks are assumed to be located in layered strata with transversely isotropy and subject to the loading of internal hydraulic pressures. For these applications, Lin and Keer (1989) attempted to quantify the crack opening displacement and the crack-front opening displacement for a vertical planar crack in a layered transversely isotropic medium. Due to the lack of an effective method for defining the angular dependence for the critical SIF, the SIFs associated with this crack problem were not given in Lin and Keer (1989). Kou and Keer (1995) further investigated the penny-shaped cracks in multilayered and isotropic solids and presented numerical values of the SIFs along the crack front.

It is well known that boundary element methods (BEM) are a powerful method for efficiently and accurately solving crack problems. Aliabadi (1997) reviewed the BEM applications in crack problems of anisotropic and composite materials. Tan and Gao (1992) employed the multi-region method and quarter-point elements of the BEM to solve several crack problems in plane orthotropic materials. Sollero and Aliabadi (1993) presented multi-region method together with a mixed-mode *J*-integral for crack problems in two-dimensional anisotropic bodies. Sollero and Aliabadi (1995) further developed a dual boundary element formulation for two-dimensional cracked bodies.

A number of investigators further incorporated the fundamental singular solutions of an infinite anisotropic solid given by Pan and Chou (1976) into the BEM for analysis of the three-dimensional crack problems. Saez et al. (1997) employed the multi-region method and singular quarter-point elements of the BEM to analyze three-dimensional crack problems in transversely isotropic bodies. Pan and Yuan (2000) developed the dual boundary element formulations and analyzed penny-shaped and square-shaped cracks in anisotropic solids. More recently, Ariza and Dominguez (2004) also developed a dual BEM formulation for analysis of three-dimensional fracture mechanics problems of transversely isotropic solids.

Evidently, when the BEM associated with Pan and Chou's solution is used for analysis of the crack problems in composites, the interfaces between different materials have to be discretized. So, some investigators attempted to use special fundamental singular solutions for analysis of the crack problems in the anisotropic composites. Pan and Amadei (1999) analyzed the fracture mechanics in two-dimensional cracked anisotropic bi-materials by the dual BEM where the fundamental singular solutions for anisotropic bi-materials were used. Yang (2002) examined the free-edge crack nucleation around an open hole in composite laminates by applying a single-domain dual BEM for multilayered composites. The fundamental singular solutions used in Yang (2002) satisfy the top- and bottom-surface boundary conditions and interfacial continuity conditions.

In the present paper, we incorporate the fundamental singular solutions given by Yue (1995) into the boundary element formulation to analyze the crack problems in two joined transversely isotropic solids. The crack problem is shown in Fig. 1. Yue's fundamental singular solutions are the problems of two joined transversely isotropic solids subject to body-forces concentrated either a point or along a circular ring, where the isotropic planes of the two materials are parallel to the plane of the material interface.

In the present BEM analysis, the conventional multi-region method is used to overcome the mathematical difficulties and avoid the numerical evaluation of the finite-part integral equations associated with the dual BEM (Pan and Amadei 1999; Yang 2002). The traction-singular elements are employed to capture the singularity around the crack front. The stress intensity factors are assessed using the crack-front opening displacements that can be obtained via the BEM.

The present BEM scheme is verified by comparing the present numerical results with the closed-form solutions for the SIFs associated with a penny-shaped crack whose surfaces are parallel to the plane of isotropy in a homogeneous and transversely isotropic solid of infinite extent. The comparison indicates that the present BEM has good accuracy. Then, the present BEM is applied to calculate the SIF values associated with a penny-shaped crack whose surfaces are perpendicular to the interface of a transversely isotropic bi-material solid and subject

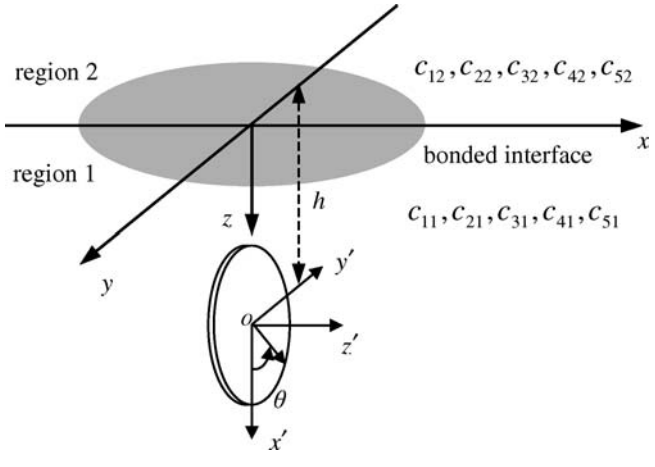

Fig. 1 A penny-shaped crack perpendicular to the bonded interface in two perfectly joined dissimilar solids with transversely isotropic properties

to the actions of three normal and one shear tractions. The SIF values of the modes I, II and III are presented for different loading conditions and different crack distances from the material interface. The data are analyzed and compared.

2 BEM for two joined transversely isotropic solids

2.1 Fundamental singular solutions for two joined transversely isotropic solids

Yue (1995) presented the closed-form fundamental singular solutions for the elastic fields of two joined transversely isotropic solids subject to concentrated point body-forces. The two solids occupy an infinite space. Their interface is planar and is perfectly bonded. The isotropic planes of the two transversely isotropic solids are parallel to the interface. The classical theory of Fourier integral transform was employed to solve the partial differential equations governing the response of the two joined transversely isotropic solids subject to the concentrated body-forces. The fundamental singular solutions of displacements and stresses are presented in the forms of the elementary harmonic functions.

The vectors of displacements $\mathbf{u} = (u_x\ u_y\ u_z)^{\mathrm{T}}$, vertical stresses $\mathbf{T}_z = (\sigma_{xz}\ \sigma_{yz}\ \sigma_{zz})^{\mathrm{T}}$ and plane strains $\mathbf{\Gamma}_p = (\varepsilon_{xx}\ \varepsilon_{xy}\ \varepsilon_{yy})^{\mathrm{T}}$ are directly obtained by Fourier integral transform. For an easy reference, the fundamental singular solutions are briefly given in the Appendix A.

The solutions for plane stresses $\mathbf{T}_p = \left(\sigma_{xx}\ \sigma_{xy}\ \sigma_{yy}\right)^{\mathrm{T}}$, vertical strains $\mathbf{\Gamma}_z = \left(\varepsilon_{xz}\ \varepsilon_{yz}\ \varepsilon_{zz}\right)^{\mathrm{T}}$ can be easily evaluated by using the results for $\mathbf{T}_z$ and $\mathbf{\Gamma}_p$ and the constitutive equation (A1).

2.2 The boundary integral equations

The numerical formulation of the BEM in two joined transversely isotropic solids using Yue's solutions can be briefly summarized in the following. When the body forces are absent, the boundary integral equations for the fundamental solutions can be expressed as follows,

$$C_{ij}(\mathbf{P})u_j(\mathbf{P}) = \int_S u^*_{ij}(\mathbf{P},\mathbf{Q})t_j(\mathbf{Q})\mathrm{d}S(\mathbf{Q}) - \int_S t^*_{ij}(\mathbf{P},\mathbf{Q})u_j(\mathbf{Q})\mathrm{d}S(\mathbf{Q}) \tag{1a}$$

where u_j and t_j are, respectively, the displacements and tractions on the boundary surface S; u^*_{ij} and t^*_{ij} are the displacements and tractions of the fundamental solutions; $\mathbf{P}$ and $\mathbf{Q}$ denote, respectively, the source and integration points on the boundaries S; and C_{ij} is a coefficient dependent on the local boundary geometry at the source point $\mathbf{P}$. The C_{ij} can be evaluated using the following equations,

$$C_{ij}(\mathbf{P}) = \lim_{\varepsilon\to 0}\int_{S_\varepsilon} t^*_{ij}(\mathbf{P},\mathbf{Q})\mathrm{d}S(\mathbf{Q}) \tag{1b}$$

where S_ε is an infinitesimal spherical surface of center $\mathbf{P}$ and radius ε enclosed in the solids. It is noted that Eq. (1a) does not contain the integration on the layer interface surface because the fundamental solution strictly satisfies the interface conditions. So, it is not necessary to have the discretization along the material interfaces in this BEM formulation. The eight-node isoparametric elements are employed to discretize the boundaries away from the crack front. Equation (1a) can be discretized to obtain a set of linear equation system for the solution of unknown boundary displacements and tractions.

Straightforward application of the BEM to the crack problems leads to the mathematical degeneration if the two crack surfaces are considered coplanar (Aliabadi 1997). The modified multi-region method (Jia et al. 1989; Yue et al. 2003) is further used here. In brief, for a crack in an infinite domain, we can form the first closed curved surface by adding an open imaginary surface in the solid to one of the crack surfaces. We can also form the second closed curved surfaces by adding the open imaginary surface in the solids to the other crack surface. The two closed curved surfaces divide the entire solids into two regions. The open imaginary surface serves a common boundary between the two regions and crack surfaces are the actual surfaces. The two regions are then joined together such that equilibrium of the tractions and compatibility of the displacements are forced on the common boundary.

2.3 Numerical methods for the crack front

As pointed out by Sih et al. (1966), the singularity of the crack front in anisotropic elastic media is the same as the one in the isotropic media. Therefore, the boundary elements of capturing the singularity around the crack front in an isotropic medium can be further employed. Several singular elements are available for modeling the behavior near the crack front. In this study, we adopted the traction-singular elements to model the singular fields around the crack front. Figure 2 illustrates the shape functions of the traction-singular elements. They can be expressed as follows (Luchi and Rizzuti 1987).

For displacements, we have:

$$N^i_d = \frac{1}{4}(1+\xi\xi_i)\left[1-\eta_i+\sqrt{2}\sqrt{1+\eta}\eta_i\right] \times \left[\xi\xi_i+\sqrt{1+\eta}\left(\sqrt{1+\eta_i}+\eta_i\right)-\xi_i\sqrt{1+\eta_i}-\xi_i(1+\eta_i)\right] \quad \text{for } i=1,2,3,4 \tag{2a}$$

$$N^i_d = \frac{1}{2}\xi_i^2(1+\xi\xi_i)\left[\left(\sqrt{2}+2\right)\sqrt{1+\eta}-\left(1+\sqrt{2}\right)(1+\eta)\right] + \frac{1}{2}\eta_i^2\left[1-\eta_i+\sqrt{2}\sqrt{1+\eta}\eta_i\right] \left(1-\xi^2\right) \text{ for } i=5,6,7,8 \tag{2b}$$

For tractions, we have:

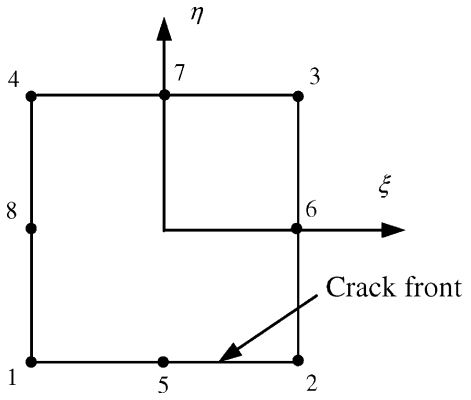

Fig. 2 A traction-singular element

$$N_t^i = \frac{1}{\sqrt{1+\eta}} N_d^i \quad \text{for } i = 1,2,5 \tag{3a}$$

$$N_t^i = \frac{\sqrt{1+\eta_i}}{\sqrt{1+\eta}} N_d^i \quad \text{for } i = 3,4,6,7,8 \tag{3b}$$

The shape functions (2) are used for the elements adjacent to a crack front on the crack faces or on the auxiliary boundary surfaces. The shape functions (3) are used only for the elements closely adjacent to the crack front on the auxiliary boundary surfaces, where the traction is singular.

Higher order singularities in the integrands can occur because of the introduction of the special shape functions in the traction-singular elements. As a result, the numerical quadrature proposed by Luchi and Rizzuti (1987) was used to solve the singular integrals. A sequence of coordinate transformations with subdivision of the singular elements was used to remove the singularities from the integrands. Nine different cases are to be dealt with in evaluating the above integrals, depending on the location of the source point **P** (taken at nodal points only). More detailed discussions on the relevant topics may be found in Luchi and Rizzuti (1987) or Yue and Xiao (2002).

2.4 Formulae for calculating the stress intensity factors

According to the work of Kassir and Sih (1966), there is an asymptotic relation between the crack opening displacements (CODs) near the crack front and the SIFs for cracked transversely isotropic media. Using the leading terms of the asymptotic relation, Ariza and Dominguez (2004) presented the formulae of the modes I, II and III SIFs in terms of the crack opening displacements at a quarter-point node of the element. In Pan and Yuan (2000), an extrapolation method of the CODs is employed for calculating the SIFs. This method also requires an asymptotically analytical expression of the crack-front CODs in terms of SIFs and can use the CODs at any point to calculate the SIFs. Owing to utilizing the extrapolation method, the high accuracy can be obtained. Herein, we employed the formulae proposed by Pan and Yuan (2000) to calculate the SIFs.

Let (x_1, x_2, x_3) be a local Cartesian co-ordinate system attached to the crack front shown in Fig. 3. The x_2-axis is normal to the crack surface, the x_3 tangential to the crack front. The x_1-axis is thus formed by the interaction of the plane normal to the crack front and the plane tangential to the crack plane. The CODs can be defined as

$$\Delta u_i(x_1,x_2,x_3) = u_i^-(x_1,x_2,x_3) - u_i^+(x_1,x_2,x_3), \quad i = 1,2,3 \tag{4}$$

where the superscripts $^+$ and $^-$ correspond to the crack surfaces whose normal directions are $n = +1$ and $n = -1$ for local co-ordinates attached to the crack front, respectively.

It is assumed that the crack front is smooth, and the leading singular term in the asymptotic expansion of the stress and displacement fields near the crack front is amenable to the generalized plane strain analysis. Therefore, the relation of the CODs at a distance r behind the crack front and the SIFs can be expressed as (Ting 1996; Suo 1990)

$$\Delta \mathbf{u} = 2\sqrt{\frac{2r}{\pi}} \mathbf{L}^{-1} \mathbf{k} \tag{5}$$

where $\Delta \mathbf{u} = (\Delta u_1, \Delta u_2, \Delta u_3)^{\mathrm{T}}$ and $\mathbf{k} = (K_{\mathrm{I}}, K_{\mathrm{II}}, K_{\mathrm{III}})^{\mathrm{T}}$ are the stress intensity factors for modes I, II and III defined as

$$K_{\mathrm{I}} = \lim_{r\to 0} \sqrt{2\pi r}\sigma_{22}(r,\theta,x_3)|_{\substack{\theta=0\\ \varphi=0}} \tag{6a}$$

$$K_{\mathrm{II}} = \lim_{r\to 0} \sqrt{2\pi r}\sigma_{12}(r,\theta,x_3)|_{\substack{\theta=0\\ \varphi=0}} \tag{6b}$$

$$K_{\mathrm{III}} = \lim_{r\to 0} \sqrt{2\pi r}\sigma_{23}(r,\theta,x_3)|_{\substack{\theta=0\\ \varphi=0}} \tag{6c}$$

Expression (5) is based on Stroh formulism. **L** is one of the Barnett-Lothe tensors (Ting 1996) which depends only on the anisotropic properties of the solids in the

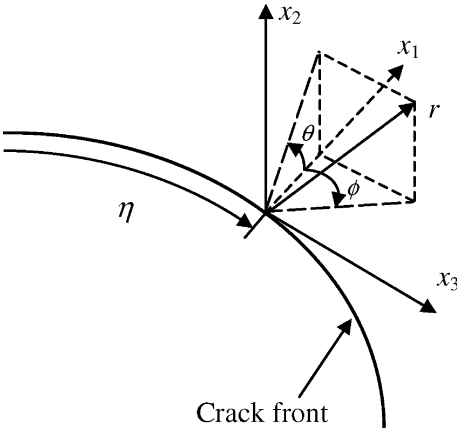

Fig. 3 Local crack-front coordinates

local crack-front coordinates. On the crack-front elements, equating the CODs from the numerical calculation to the analytical expression (5), one then obtains a set of algebraic equations from which the SIFs, K_{I}, K_{II} and K_{III}, can be solved.

3 Numerical examples

3.1 Material properties

Assume that the x-y plane is the plane of isotropy for a transversely isotropic solid with the z-axis being the axis of material symmetry. We introduced the following elastic constants: E_x, μ_x, v_{xy} and E_z, μ_z, v_{xz}. The E_x, μ_x and v_{xy} are the Young's modulus, shear modulus and Poisson's ratio in the x-y plane of isotropy, respectively. The E_z, μ_z and v_{xz} are those quantities in the transverse direction z. The five elastic moduli $c_{ik}(i = 1, 2, 3, 4, 5; k = 1, 2)$ in formulae (A1) can be related to the above-mentioned elastic constants as

$$c_{1k} = 2\mu_x\left(1 - v_{xz}^2 E_x/E_z\right)/\left(1 - v_{xy} - 2v_{xz}^2 E_x/E_z\right) \tag{7a}$$

$$c_{2k} = E_x v_{xz}/\left(1 - v_{xy} - 2v_{xz}^2 E_x/E_z\right) \tag{7b}$$

$$c_{3k} = E_z\left(1 - v_{xy}\right)/\left(1 - v_{xy} - 2v_{xz}^2 E_x/E_z\right) \tag{7c}$$

$$c_{4k} = \mu_z \tag{7d}$$

$$c_{5k} = \mu_x = E_x/2\left(1 + v_{xy}\right) \tag{7e}$$

For an isotropic material, the five elastic constants are degenerated into two elastic constants as follows,

$$c_{1k} = c_{3k} = \lambda + \mu, \quad c_{2k} = \lambda, \quad c_{4k} = c_{5k} = \mu. \tag{8}$$

where λ and μ are the Lame's constants for an isotropic material.

As shown in Table 1, four sets of the transversely isotropic materials (TI-1, 2, 3, 4) are selected for numerical evaluation. Pan et al. (1996, 2000) and Hoenig (1978) selected the similar elastic constants of the TI-1 and TI-2 materials. Lin and Keer (1989) and Kassir and Sih (1975) selected the elastic constants of the TI-3 and TI-4 materials. In Yue (1995), the elastic constants for the TI-3 and TI-4 materials were also used. Consequently, we have the following eight cases of material combination for the two bonded solids of an infinite extent, shown in Table 2. Note that the cracks are always located in region 1 ($z \geq 0^+$) for all the cases under consideration.

Table 2 Cases of two joined transversely isotropic solids

Cases	$z \geq 0^+$	$z \leq 0^-$	Note
1	TI-1	TI-1	a homogeneous solid
2	TI-2	TI-2	a homogeneous solid
3	TI-1	TI-2	two joined bi-materials
4	TI-2	TI-1	two joined bi-materials
5	TI-3	TI-3	a homogeneous solid
6	TI-4	TI-4	a homogeneous solid
7	TI-3	TI-4	two joined bi-materials
8	TI-4	TI-3	two joined bi-materials

3.2 Loading conditions

We considered two kinds of cracks whose surfaces are parallel or perpendicular to the plane of isotropy of a transversely isotropic solid. The crack surfaces are subject to normal or shear tractions. The crack surfaces are subject to the normal tension p and the shear q on the crack surfaces respectively, i.e.,

$$\sigma_{z'z'}^{+} = \sigma_{z'z'}^{-} = -p, \ p \geq 0 \tag{9a}$$

$$\sigma_{x'y'}^{+} = \sigma_{x'y'}^{-} = 0 \tag{9b}$$

$$\sigma_{x'z'}^{+} = \sigma_{x'z'}^{-} = -q, \ q \geq 0 \tag{9c}$$

where $0 \leq r < a$ (crack radius a), and the superscripts $^+$ and $^-$ correspond to the crack surfaces whose normal directions are $n = +1$ and $n = -1$, respectively. Furthermore, the x', y' and z' are local coordinates attached to the crack surfaces (Fig.1). Several loading conditions are analyzed as follows,

$$q = q_0 \tag{10a}$$

$$p = p_0, \ p_0(r/a), \ p_0(r/a)^2 \tag{10b}$$

where p_0 and q_0 are constants, and the r is the distance of any point on the crack surface from the origin in the local coordinate. Ozturk and Erdogan (1996) also considered the above three normal tensions in formula (10b) for penny-shaped cracks in the functionally graded materials.

In the ensuing, we firstly verified the accuracy and efficiency of the proposed method by comparing the existing analytical and numerical solutions for the penny-shaped cracks parallel to the plane of isotropy in a transversely isotropic solid. Then, we presented the SIF values of penny-shaped cracks perpendicular to the plane of isotropy in two joined transversely isotropic solids and subject to different normal loads and uniform shear traction (Fig. 1).

Table 1 The elastic constants of the four materials

Material types	Elastic constants
Class I material (TI-1)	$E_x/E_z = 3$, $v_{xy} = 0.25$, $\mu_z = 0.25$, $\mu_z/E_z = 0.4$.
Class II material (TI-2)	$E_x/E_z = 0.5$, $v_{xy} = 0$, $\mu_z = 0.4$, $\mu_z/E_z = 0.8$.
Class III material (TI-3)	$c_1 = 41.19$, $c_2 = 14.97$, $c_3 = 42.57$, $c_4 = 11.32$, $c_5 = 11.56kPa$.
Class IV material (TI-4)	$c_1 = 111.02$, $c_2 = 34.57$, $c_3 = 42.09$, $c_4 = 26.43$, $c_5 = 43.59kPa$.

4 Numerical verification

We consider a penny-shaped crack whose surfaces are parallel to the plane of isotropy in a transversely isotropic solid of infinite extent. The crack surfaces are subject to the uniform tension $p = p_0$. Evidently, the cracked body is of symmetry to the $x'oz'$-plane. So, the BEM formulation of the crack problem is carried out by examining the left symmetrical part of the entire crack geometry.

For convenience, we choose a hemisphere in a homogeneous material to form the two regions for the BEM analysis. Because of symmetry, it is necessary only to analyze half of the hemisphere. We only discretize this half hemisphere. We do not need to discretize the plane of the symmetry into BEM meshes. Figure 4 shows the discretized left symmetrical surface with 553 nodes and 176 elements. We use 32 traction-singular elements along the crack front. The boundary element mesh has been employed for analysis of the crack problems in functionally graded materials (Xiao et al. 2005).

For the uniform tension on crack surfaces ($p = p_0$) and the crack surfaces parallel to the plane of isotropy of a homogeneous and transversely isotropic medium, the mode I stress intensity factor is $K_I = 2p_0\sqrt{a/\pi}$ (Hoenig 1978). It should be noted that for penny-shaped or elliptical cracks whose surfaces are parallel to the plane of isotropy of a transversely isotropic medium and subject to the uniform tension, the SIF values in an infinite isotropic solid is independent of the material property. For cases 1 and 2, numerical results of the normalized mode I SIFs ($K_I/p_0\sqrt{\pi a}$) along the crack front vary from 0.63 to 0.64, compared with the value $2/\pi \approx 0.6366$ in the analytical solutions. The largest derivation for the SIFs using the BEM is less than 1 per cent.

For the uniform shear on crack surfaces ($q = q_0$) and the crack surfaces parallel to the plane of isotropy of a transversely isotropic medium, the modes II and III stress intensity factors are related to elastic constants and presented as follows (Hoenig 1978),

$$K_I = 0 \tag{11a}$$

$$K_{II} = q_0\sqrt{\pi a}\cos\theta/R_1 \tag{11b}$$

$$K_{III} = -q_0\sqrt{\pi a}S\cos\theta/(TR_1) \tag{11c}$$

where

$$S = \sqrt{\left(1 - v_{xy}^2\right)/2} \times \sqrt{(1 + v_{xy})(\mu_x/\mu_z - v_{xz}) + \sqrt{\left(1 - v_{xy}^2\right)E_x/E_z - v_{xz}^2}} \tag{11d}$$

$$T = \left(1 + v_{xy}\right)\sqrt{\mu_x/\mu_z} \tag{11e}$$

$$R_1 = \pi(1 + S/T)/4 \tag{11f}$$

The numerical and analytical solutions for case 1 are shown in Fig. 5. The maximum difference between the analytical and numerical solutions of the normalized mode II SIFs ($K_{II}/p_0\sqrt{\pi a}$) is 0.5% whilst the one between the analytical and numerical solutions of the normalized mode III SIFs ($K_{III}/p_0\sqrt{\pi a}$) is about 1.4%. It may be found that the results obtained from the numerical method are in very good agreement with analytical solutions.

5 Numerical results and discussions

We now apply the BEM to solve the penny-shaped crack problems in the transversely isotropic bi-material solid as shown in Fig. 1. The material properties and the loading conditions are given in Sect. 3 above. We will have four loading cases. We will present and discuss the

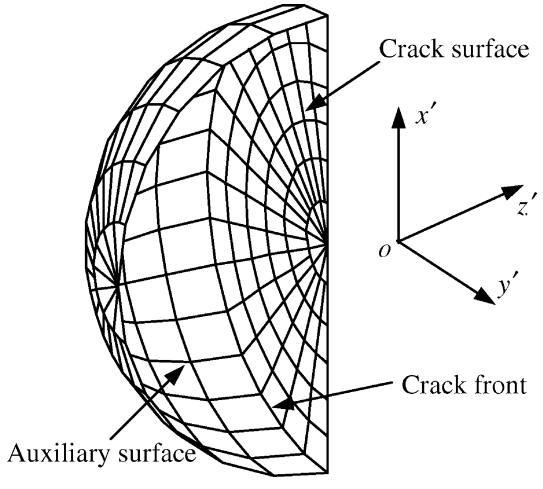

Fig. 4 Boundary element mesh of the crack body

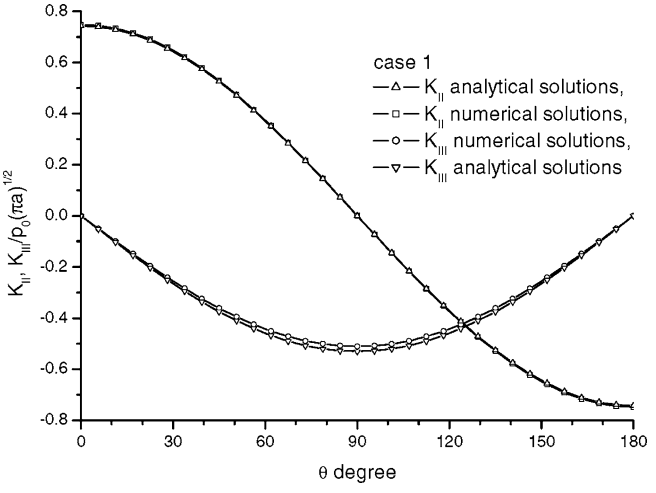

Fig. 5 Comparison of the SIFs ($K_{II}/q_0\sqrt{\pi a}, K_{III}/q_0\sqrt{\pi a}$) of the crack parallel to the plane of isotropy between the numerical and analytical solutions for case 1 and $q = q_0$

SIF values for the crack front associated with the four loading cases below.

5.1 The crack surfaces are subject to the uniform tension $p = p_0$

At first, we consider the penny-shaped cracks perpendicular to the plane of isotropy in two joined transversely isotropic solids and subject to the uniform tension $p = p_0$. The examples consider penny-shaped cracks located in region 1 at a distance h from the bi-material interface. For the cases, the cracked body also is symmetric with respect to the $x'oz'$-plane (see Fig. 1). Thus, the boundary element mesh shown in Fig. 4 can be used to analyze the crack problems. The normalized SIF values ($K_I/p_0\sqrt{\pi a}$) for this loading ($p = p_0$) are presented in Figs. 6a–d and Table 3.

For crack problems in a homogenous and transversely isotropic medium, i.e., case 1 and case 2, the stress intensity factors are shown in Figs. 6a and 6b. The mode I SIF values along the crack front are symmetric with the plane $y'oz'$. In Figs. 6a and 6b, it can be found that the anisotropy of the materials exerts an obvious influence on the SIFs. Note that the mode I SIFs in a homogenous and isotropic medium is $K_I/p_0\sqrt{\pi a} = 2/\pi$ along the crack front. It is interesting that for the case of the crack surfaces perpendicular to the plane of the isotropy, the SIF values vary along the crack front. The similar phenomena are also found in Hoenig (1978), Pan and Yuan (2000).

Figure 6a also shows the variations of the normalized SIFs ($K_I/p_0\sqrt{\pi a}$) along the crack front with the crack distances from the material interface for case 1 and case 3. It can be found that the material in region 2 exerts a weak influence on the SIFs along the crack front in $\theta \in [90°, 180°]$ and the effect of region 2 on the SIFs along the crack front in $\theta \in [0°, 90°]$ is not obvious. With the crack distances from the material interface decreasing, the SIFs along the crack front around $\theta = 180°$ increase slowly.

Figure 6b also illustrates the variations of the normalized SIFs ($K_I/p_0\sqrt{\pi a}$) along the crack front with the crack distances from the material interface for case 2 and case 4. It can be found that the material of region 2 exerts an obvious influence on the SIFs along the crack

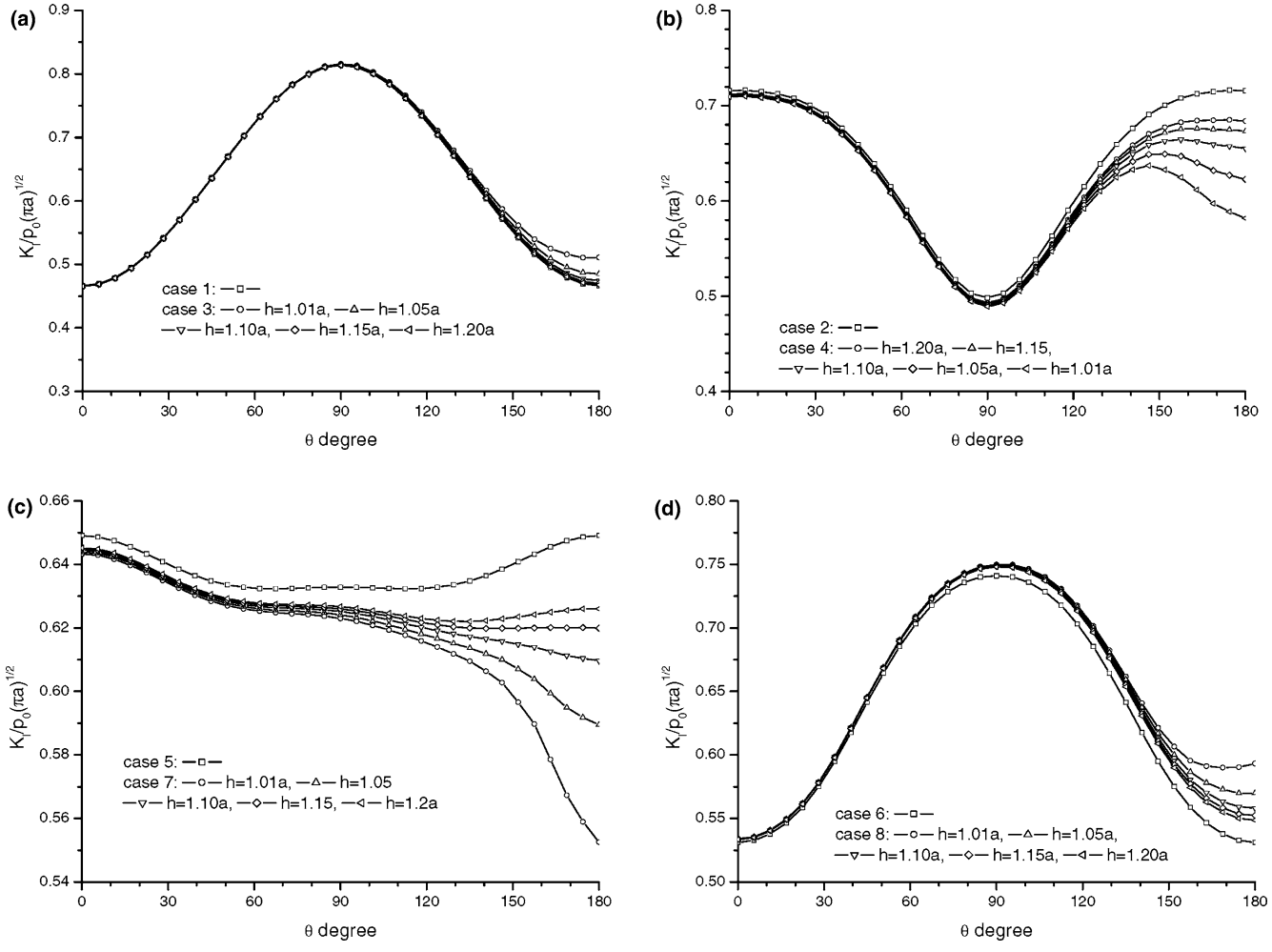

Fig. 6 Variation of the SIFs ($K_I/p_0\sqrt{\pi a}$) with the crack distance from the material interface $p = p_0$

Table 3 Variations of the SIFs ($K_I/p_0\sqrt{\pi a}$) for the eight cases, $p = p_0$

θ degree	Case 1	Case 3		Case 2	Case 4		Case 5	Case 7		Case 6	Case 8	
		$h = 1.01a$		$h = 1.2a$		$h = 1.01a$	$h = 1.2a$		$h = 1.01a$	$h = 1.2a$		$h = 1.01a$	$h = 1.2a$
90.00	0.814364	0.815765	0.8136	0.49832	0.489147	0.493119	0.632851	0.622983	0.626689	0.741025	0.749874	0.747965	
112.50	0.761588	0.766172	0.761397	0.563141	0.547047	0.554649	0.632329	0.617712	0.623798	0.717852	0.730776	0.727147	
135.00	0.637065	0.647633	0.637575	0.65922	0.624607	0.64375	0.634761	0.609525	0.622022	0.641394	0.661703	0.653681	
157.50	0.515891	0.53993	0.516903	0.708049	0.624772	0.682393	0.643241	0.589701	0.624218	0.558755	0.59545	0.574327	
180.00	0.466553	0.510983	0.467763	0.715752	0.581832	0.683984	0.649098	0.552599	0.626033	0.530992	0.593215	0.548696	

front in $\theta \in [90°, 180°]$ and has relatively weak influence on the SIFs along the crack front in $\theta \in [0°, 90°]$. With the crack distances from the material interface decreasing, the SIFs along the crack front around $\theta = 180°$ decrease.

Figures 6c and 6d present the variations of normalized SIF ($K_I/p_0\sqrt{\pi a}$) along the crack front for case 5 and case 6. For case 5, the SIFs are close to the ones of the crack in an isotropic medium. This is because the elastic parameters of the material TI-3 are approximate to those of an isotropic medium. For case 6, the anisotropy of the material TI-4 exerts an obvious influence on the SIFs along the crack front.

Figure 6c also shows the variations of the normalized SIFs ($K_I/p_0\sqrt{\pi a}$) along the crack front with the crack distances from the materials for case 6 and case 7. It can be found that the SIFs become small because of the existence of the material in region 2. The variations of the SIFs are obvious in $\theta \in [90°, 180°]$. And the influence of region 2 on the SIFs is relative weak in $\theta \in [0°, 90°]$. With the crack distances from the material interface decreasing, the influence becomes more obvious, especially for the crack front around $\theta = 180°$.

Figure 6d also shows the variations of the normalized SIFs ($K_I/p_0\sqrt{\pi a}$) along the crack front with the crack distances from the material interface for case 6 and case 8. It can be found that the SIFs become larger than the ones in the homogeneous medium (case 6) with the crack distances from the material interface decreasing. The variations of the SIFs are more obvious in $\theta \in [90°, 180°]$ than in $\theta \in [0°, 90°]$.

Evidently, the above variations of the SIFs along the crack front are due to the existence of material in region 2. For region 2 having a stiffer material than region 1, region 2 tends to constrain the crack opening and the SIFs decrease. And for region 2 having a more complaint material than region 1, region 2 tends to make the crack opening easy and the SIFs increase.

5.2 The crack surfaces are subject to the triangle tension $p = p_0(r/a)$

Secondly, we consider the penny-shaped cracks perpendicular to the plane of isotropy in two joined transversely isotropic solids and subject to the normal tension $p = p_0(r/a)$. For the cases, the cracked body also is symmetric with respect to the $x'oz'$-plane (see, Fig. 1). Thus, the boundary element mesh shown in Fig. 4 can further be used to analyze the crack problems. The normalized SIF values ($K_I/p_0\sqrt{\pi a}$) for the loading $p = p_0$ are presented in Figs. 7a–d and Table 4.

In these tables and figures, it can be found that the loading $p = p_0(r/a)$ causes the similar variations of the SIFs to $p = p_0$ along the crack front with the crack distances from the material interface for the eight cases. Table 6 presents a comparison of the results for $p = p_0$

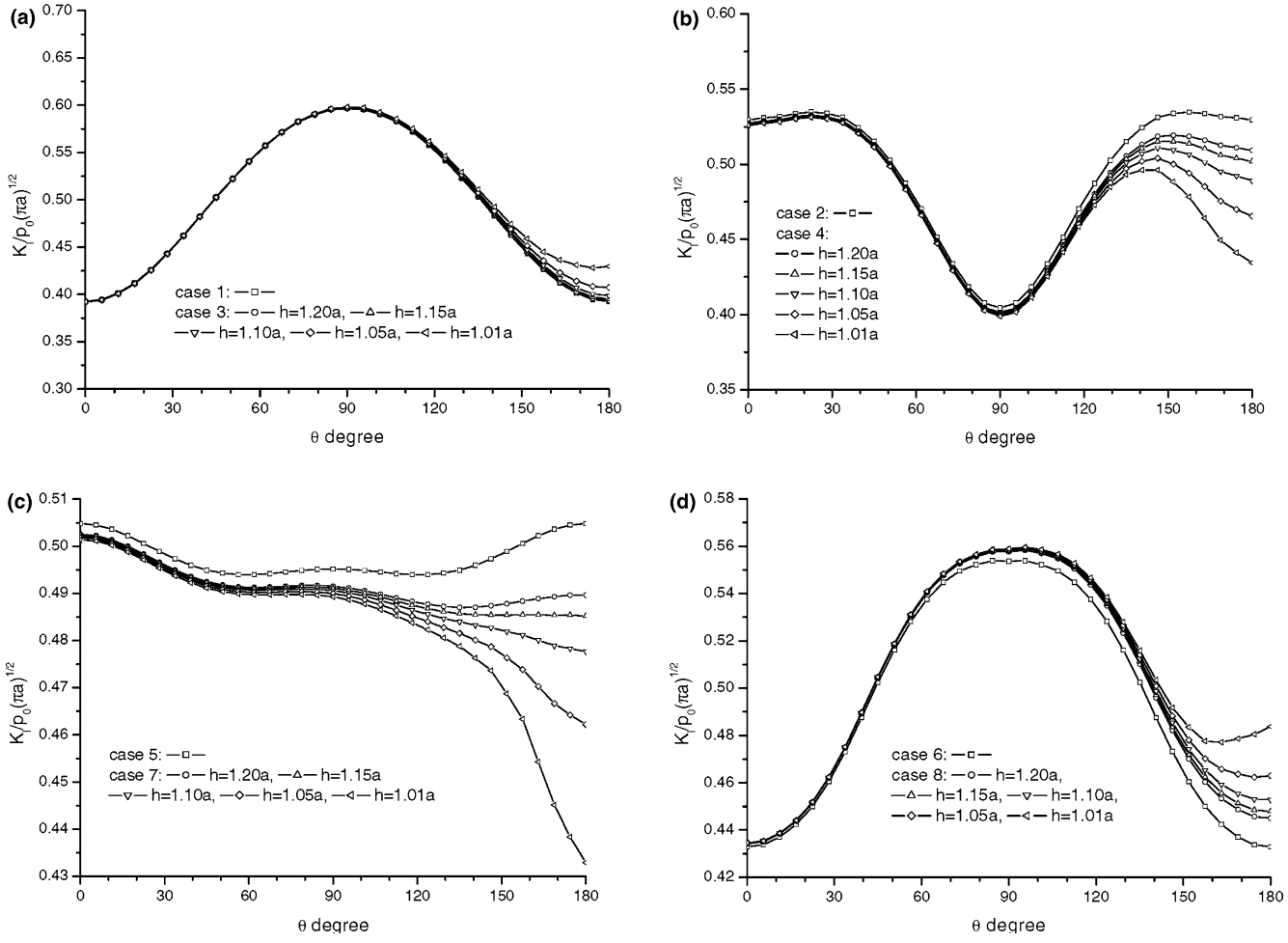

Fig. 7 Variation of the SIFs ($K_I/p_0\sqrt{\pi a}$) with the crack distance from the material interface $p = p_0(r/a)$

and $p = p_0(r/a)$ at the crack front $\theta = 180°$. These data are obtained by the following formula for the same loading, [$K_I/p_0\sqrt{\pi a}$ for a transversely isotropic solid – $K_I/p_0\sqrt{\pi a}$ for two joined transversely isotropic solids] %.

It can be found that the absolute increments in Table 6 decrease from $p = p_0$ to $p = p_0(r/a)$ for the same crack distance to the material interface. This indicates that the effects of materials in region 2 on the SIFs become weak with the load on the crack surfaces decreasing.

5.3 The crack surfaces are subject to the circular tension $p = p_0(r/a)^2$

Thirdly, we consider the penny-shaped cracks perpendicular to the plane of isotropy in two joined transversely isotropic solids and subject to the normal tension $p = p_0(r/a)^2$. For the cases, the cracked body also is symmetric with respect to the $x'oz'$-plane (see Fig. 1). Thus, the boundary element mesh shown in Fig. 4 can further be used to analyze the crack problems. The normalized SIF values ($K_I/p_0\sqrt{\pi a}$) for the loading $p = p_0$ are presented in Figs. 8a–d and Tables 5.

In these tables and figures, it can also be found that the loading $p = p_0(r/a)^2$ induces the similar variations of

Table 4 Variations of the SIFs ($K_I/p_0\sqrt{\pi a}$) for the eight cases, $p = p_0(r/a)$

θ degree	Case 1	Case 3		Case 2	Case 4		Case 5	Case 7		Case 6	Case 8	
		$h = 1.01a$	$h = 1.2a$		$h = 1.01a$	$h = 1.2a$		$h = 1.01a$	$h = 1.2a$		$h = 1.01a$	$h = 1.2a$
90.00	0.5967	0.59785	0.59625	0.404425	0.398865	0.40128	0.49518	0.48927	0.49152	0.5537	0.55895	0.55775
112.50	0.57175	0.57515	0.5717	0.45136	0.44148	0.44626	0.4942	0.48526	0.48904	0.5448	0.5528	0.55045
135.00	0.5031	0.51085	0.50355	0.51515	0.493125	0.50555	0.494915	0.47878	0.48702	0.5024	0.5159	0.5102
157.50	0.42624	0.444915	0.427105	0.5348	0.478255	0.51855	0.5006	0.46333	0.48835	0.45007	0.47762	0.460385
180.00	0.3925	0.429455	0.39352	0.52945	0.434415	0.50915	0.5048	0.432915	0.489645	0.43289	0.48379	0.445

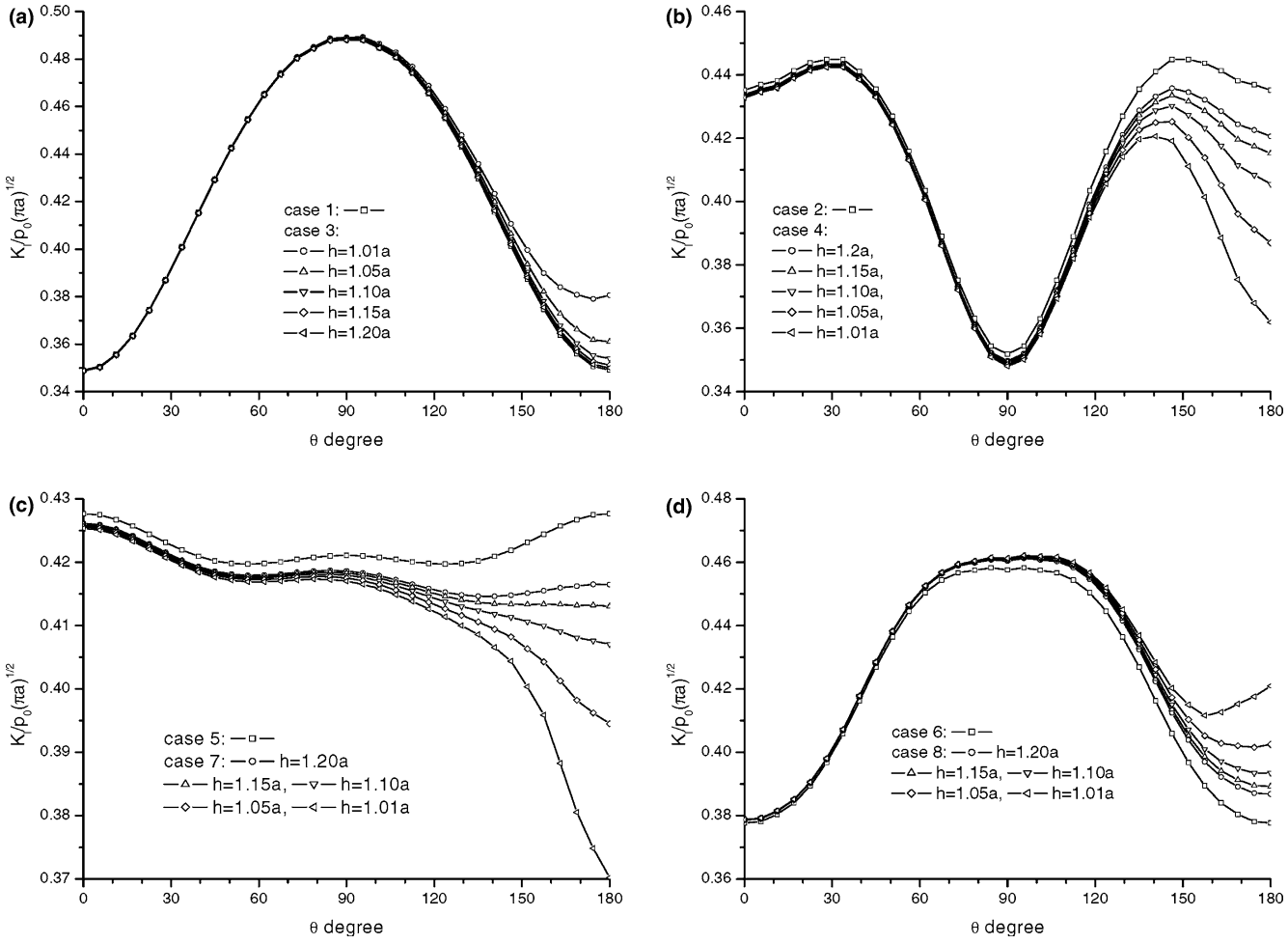

Fig. 8 Variation of the SIFs ($K_I/p_0\sqrt{\pi a}$) with the crack distance from the material interface $p = p_0(r/a)^2$

the SIFs to $p = p_0$ and $p = p_0(r/a)$ along the crack front with the crack distances from the material interface for the eight cases. Table 6 also presents a comparison of the results for $p = p_0$ and $p = p_0(r/a)$, $p = p_0(r/a)^2$ at the crack front $\theta = 180°$. It can be found that the absolute increments of the SIFs in Table 6 decrease from $p = p_0$, $p = p_0(r/a)$ to $p = p_0(r/a)^2$ for the same crack distance to the material interface. This further verifies the above conclusion that the effect of the material in region 2 on the SIFs becomes weak with the load on the crack surfaces decreasing.

5.4 The crack surfaces are subject to the uniform shear traction

Lastly, we consider the SIF values of the crack perpendicular to the material interface and subject to shear traction $q = q_0$. For such uniform shear loading, the mode II and mode III SIF values are non-zero while the mode I SIF values are always zero. If the crack is in a homogeneous and isotropic solid and is subject to the uniform shear, the analytical solutions of the two mode SIFs are in very agreement with the numerical solution. These two solutions are shown in Figs. 9 and 10.

Table 5 Variations of the SIFs ($K_I/p_0\sqrt{\pi a}$) for the eight cases, $p = p_0(r/a)^2$

θ degree	Case 1	Case 3		Case 2	Case4		Case 5	Case 7		Case 6	Case 8	
		$h = 1.01a$	$h = 1.2a$		$h = 1.01a$	$h = 1.2a$		$h = 1.01a$	$h = 1.2a$		$h = 1.01a$	$h = 1.2a$
90.00	0.4882	0.48915	0.48795	0.35189	0.34808	0.34973	0.4211	0.41701	0.41861	0.45763	0.46122	0.4604
112.50	0.47402	0.47674	0.47411	0.38892	0.382	0.38535	0.42007	0.41381	0.41653	0.45439	0.46000	0.45831
135.00	0.42971	0.43586	0.43019	0.4355	0.41967	0.42873	0.4202	0.40858	0.41461	0.42693	0.43692	0.43248
157.50	0.37468	0.38993	0.37544	0.44374	0.40143	0.43212	0.42441	0.39589	0.41551	0.3894	0.41161	0.39703
180.00	0.34917	0.38067	0.35002	0.43522	0.36192	0.42063	0.42766	0.37022	0.4165	0.37768	0.42098	0.38684

Table 6 Comparison of the SIFs ($K_I/p_0\sqrt{\pi a}$) among three different loadings at $\theta = 180°$

h	Case 3			Case 4			Case 7			Case 8		
	p_0	$p_0(r/a)$	$p_0(r/a)^2$	p_0	$p_0(r/a)$	$p_0(r/a)^2$	p_0	$p_0(r/a)$	$p_0(r/a)^2$	p_0	$p_0(r/a)$	$p_0(r/a)^2$
1.01a	4.44	3.70	3.15	−13.39	−9.50	−7.33	−9.65	−7.19	−5.74	6.22	5.10	4.33
1.05a	1.86	1.46	1.19	−9.32	−6.40	−4.82	−5.96	−4.26	−3.31	3.88	3.01	2.48
1.10a	0.78	0.60	0.48	−6.07	−4.03	−2.96	−3.94	−2.72	−2.06	2.71	1.99	1.58
1.15a	0.37	0.26	0.21	−4.25	−2.77	−2.00	−2.92	−1.96	−1.46	2.13	1.51	1.16
1.20a	0.12	0.10	0.09	−3.18	−2.03	−1.46	−2.31	−1.52	−1.12	1.77	1.21	0.92

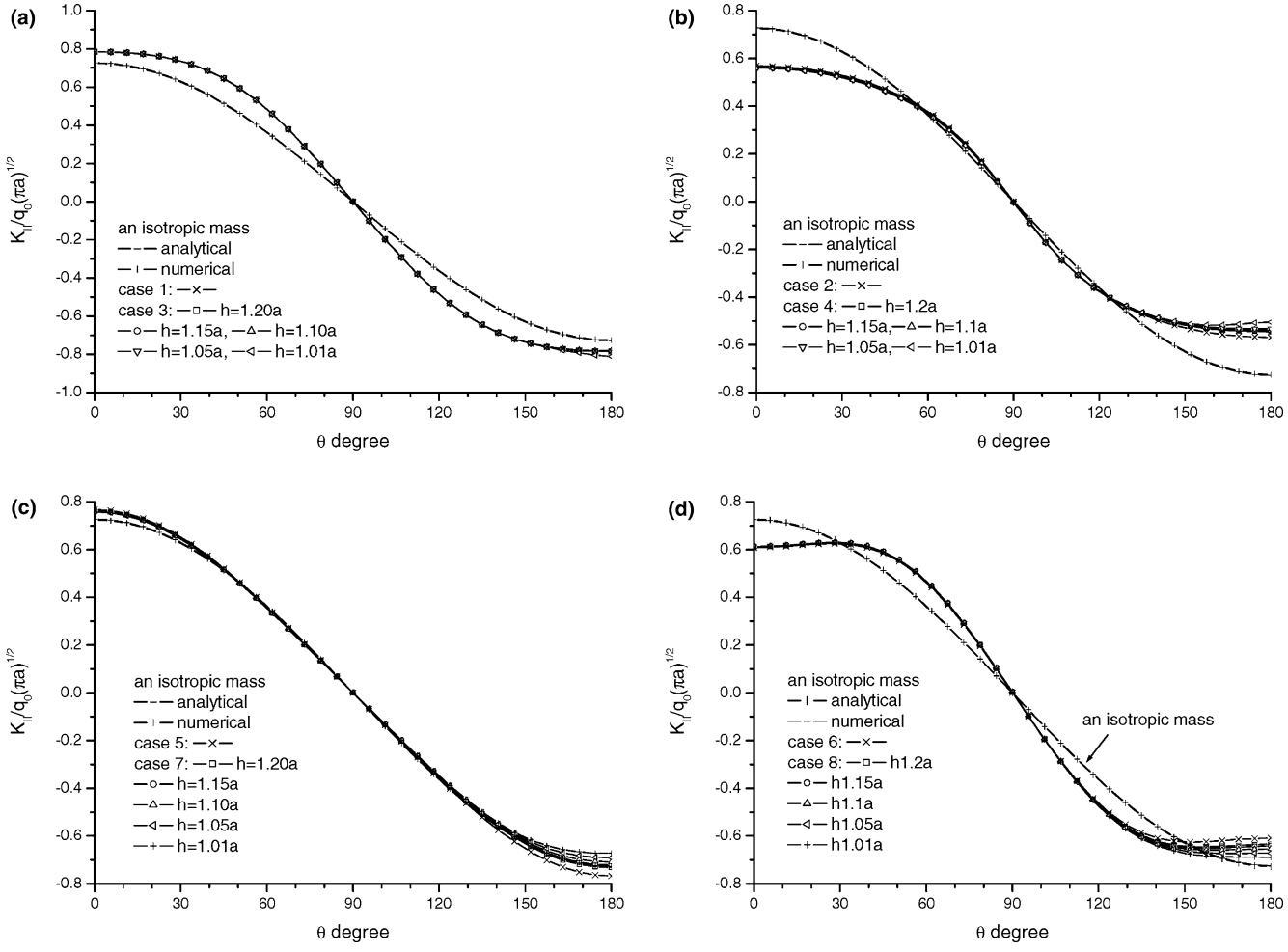

Fig. 9 Variation of the SIFs ($K_{II}/p_0\sqrt{\pi a}$) with the crack distance from the material interface, $q = q_0$

5.4.1 The mode II SIF values

The mode II SIF values are given in Fig. 9 and Table 7. Obviously, the magnitudes of SIF values in a transversely isotropic mass are different from the ones in an isotropic mass. For case 1 and case 5, the absolute SIF values are less than the ones in an isotropic mass. For cases 2 and 6, the absolute SIF values decrease in the neighborhood of $\theta = 0°$ and 180° and increase in the neighborhood of $\theta = 90°$ (excluding $\theta = 90°$). It can be found that region 2 exerts more obvious influence on the SIF values near $\theta = 180^0$ than $\theta = 0°$. And for case 3 and case 8, the absolute SIF values increase and for case 4 and case 5, the absolute SIF values decrease near $\theta = 0°$ and $\theta = 180°$.

5.4.2 The mode III SIF values

The mode II SIF values are given in Fig. 10 and Table 8. By comparing the SIF values in the isotropic and transversely isotropic solids, it can be found the transversely isotropic properties strongly effects the SIF values. Due to symmetry of the geometric and loading conditions, the SIF values at $\theta = 0°$ and $\theta = 180°$ are equal to zero and the maximum absolute values of the SIFs appear at $\theta = 90°$. Thus, region 2 has an obvious

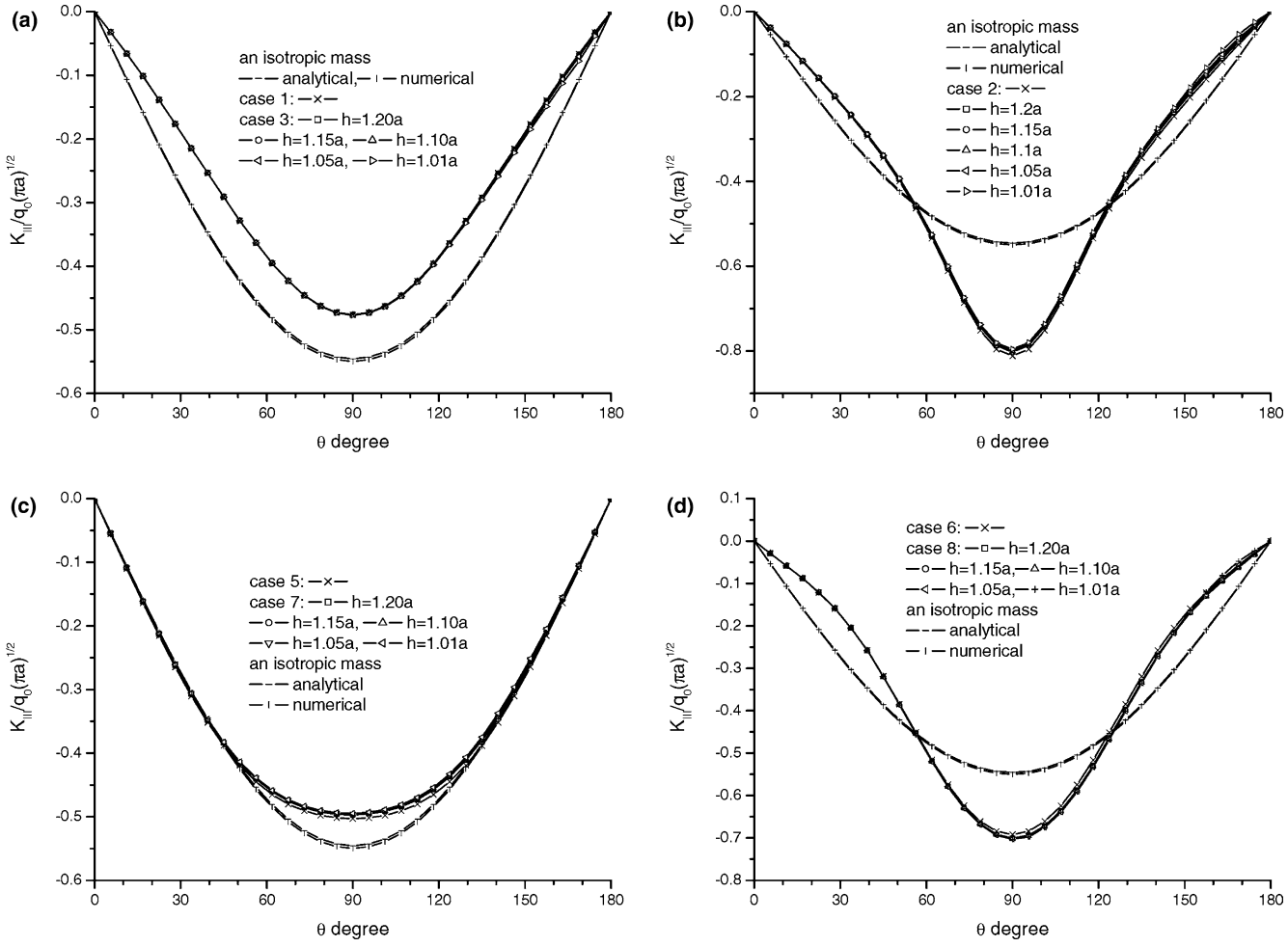

Fig. 10 Variation of the SIFs ($K_{III}/p_0\sqrt{\pi a}$) with the crack distance from the material interface, $q = q_0$

influence on the SIF in the neighborhood of $\theta = 90°$. The effect of region 2 on the mode III SIFs are similar to the ones on the mode II SIFs. For case 3 and case 8, the absolute SIF values of mode III increase and for case 4 and case 5, the absolute SIF values of mode III decrease.

6 Summary and Conclusions

In the above, we have incorporated Yue's fundamental singular solutions into the classic displacement boundary integral equation formulations. The modified multi-region method of the BEM and the traction singular elements are employed to analyze the penny-shaped crack problems in two joined transversely isotropic solids. The two orientations of the penny-shaped cracks are discussed, i.e., the crack surfaces are parallel and perpendicular to the isotropic plane of transversely isotropic solids. The cases of the cracks parallel to the isotropic plane of the transversely isotropic solid are employed to verify the accuracy of the proposed method by comparing the existing analytical solutions in a homogenous and transversely isotropic solid. The results show that the numerical results obtained by the present BEM are in very good agreement with the closed-from solutions.

Table 7 Variations of the SIFs ($K_{\rm II}/q_0\sqrt{\pi a}$) for the eight cases, $q = q_0$

θ degree	Case 1	Case 3		Case 2	Case4		Case 5	Case 7		Case 6	Case 8	
		$h = 1.01a$	$h = 1.2a$		$h = 1.01a$	$h = 1.2a$		$h = 1.01a$	$h = 1.2a$		$h = 1.01a$	$h = 1.2a$
90.00	0.00034	−0.00014	−0.00084	0.000305	−0.00394	−0.0021	0.000229	0.000907	0.0002	0.000348	0.002807	0.003487
112.50	−0.37869	−0.37908	−0.37957	−0.3082	−0.30738	−0.30749	−0.27035	−0.2633	−0.26641	−0.36839	−0.37527	−0.37063
135.00	−0.64484	−0.64461	−0.64502	−0.47227	−0.46408	−0.46704	−0.52072	−0.49855	−0.50913	−0.58577	−0.61123	−0.59703
157.50	−0.76122	−0.76145	−0.76032	−0.54676	−0.51746	−0.5312	−0.70191	−0.63999	−0.6765	−0.62366	−0.68301	−0.64511
180.00	−0.78446	−0.81048	−0.78259	−0.56863	−0.50477	−0.5443	−0.7675	−0.67138	−0.7321	−0.60844	−0.68925	−0.63445

Table 8 Variations of the SIFs ($K_{III}/q_0\sqrt{\pi a}$) for the eight cases, $q = q_0$

θ degree	Case 1	Case 3		Case 2	Case4		Case 5	Case 7		Case 6	Case 8	
		$h = 1.01a$	$h = 1.2a$		$h = 1.01a$	$h = 1.2a$		$h = 1.01a$	$h = 1.2a$		$h = 1.01a$	$h = 1.2a$
90.00	−0.47645	−0.47699	−0.47619	−0.81142	−0.79576	−0.80253	−0.50298	−0.49461	−0.49721	−0.69211	−0.70321	−0.70027
112.50	−0.42352	−0.42508	−0.42344	−0.61159	−0.59689	−0.60329	−0.48027	−0.46982	−0.47316	−0.57462	−0.59117	−0.58663
135.00	−0.29164	−0.296	−0.29206	−0.34433	−0.32817	−0.3361	−0.38828	−0.37479	−0.3798	−0.31919	−0.33464	−0.33113
157.50	−0.13913	−0.14933	−0.13985	−0.15878	−0.13243	−0.15062	−0.2157	−0.20452	−0.20842	−0.12178	−0.12034	−0.12954
180.00	−0.0001	−0.00011	−0.0001	−0.00014	−0.00012	−0.00013	−0.00019	−0.00017	−0.00018	−0.00008	−9.1E−05	−8.3E−05

The cases of the cracks perpendicular to the isotropic plane of the two joined transversely isotropic solids are used to illustrate the influence of the anisotropy on the SIFs for three different normal tractions and the shear traction. The four transversely isotropic materials and the eight cases of the two joined transversely isotropic solids are considered. From the numerical solutions, there is an evident influence of the material anisotropy on the SIFs. Owing to the existence of another half-space transversely isotropic solid, there are clear variations of the SIFs along the crack front, especially for the crack front near another transversely isotropic solids.

The examples presented in the paper have shown that the new BEM can be used to efficiently and accurately carry out the analysis and prediction of the penny-shaped crack problems in the two joined transversely isotropic solids. Besides, a quite large amount of SIF values are presented and would be useful for furthering our knowledge on fracture mechanics of the two joined transversely isotropic solids.

Appendix A

For a transversely isotropic bi-material solid with the z-axis being the axis of material symmetry, x-y plane is the plane of isotropy, shown in Fig. 1. The constitutive relation between the stress σ_{ij} and the strain ε_{ij} can be expressed in terms of the contracted stiffness matrix as

$$\begin{bmatrix}\sigma_{xx}\\ \sigma_{yy}\\ \sigma_{zz}\\ \sigma_{yz}\\ \sigma_{xz}\\ \sigma_{xy}\end{bmatrix} = \begin{bmatrix} c_{1k} & c_{1k}-2c_{5k} & c_{2k} & 0 & 0 & 0\\ c_{1k}-2c_{5k} & c_{1k} & c_{2k} & 0 & 0 & 0\\ c_{2k} & c_{2k} & c_{3k} & 0 & 0 & 0\\ 0 & 0 & 0 & 2c_{4k} & 0 & 0\\ 0 & 0 & 0 & 0 & 2c_{4k} & 0\\ 0 & 0 & 0 & 0 & 0 & 2c_{5k}\end{bmatrix} \times \begin{bmatrix}\varepsilon_{xx}\\ \varepsilon_{yy}\\ \varepsilon_{zz}\\ \varepsilon_{yz}\\ \varepsilon_{xz}\\ \varepsilon_{xy}\end{bmatrix} \tag{A1}$$

where c_{1k}, c_{2k}, c_{3k}, c_{4k} and c_{5k} are the five elastic constants for the k-th transversely isotropic solid of the by-material system, where $k = 1$ for $0^+ \le z < \infty$ or 2 for $-\infty < z \le 0^-$.

The vectors of displacements, vertical stresses and plane strains are, respectively, defined by

$$\mathbf{u} = \left(u_x\ u_y\ u_z\right)^{\mathrm{T}},\ \mathbf{T}_z = \left(\sigma_{xz}\ \sigma_{yz}\ \sigma_{zz}\right)^{\mathrm{T}},\ \boldsymbol{\Gamma}_p = \left(\varepsilon_{xx}\ \varepsilon_{xy}\ \varepsilon_{yy}\right)^{\mathrm{T}} \tag{A2}$$

Without loss of generality, we assume that the body forces are in the solid of half region $k = 1$, i.e. $h \ge 0^+$. The vector of a concentrated body forces is located at $(0, 0, h)$ and defined by

$$\mathbf{F} = \left(F_x, F_y, F_z\right)^{\mathrm{T}} \tag{A3}$$

And the field point is located at (x, y, z). The solutions for four different cases are presented in the ensuing. Let $\Delta_k = \sqrt{c_{1k}c_{3k}} - c_{2k} - 2c_{4k}$, and Δ_{1k} and Δ_{2k} correspond to two different transversely isotropic solids, respectively. By using the classical Fourier transform techniques, Yue (1995) developed the fundamental solutions for the elastic fields in two joined transversely isotropic solids subject to concentrated point forces. The fundamental solutions of displacements and stresses are presented in the forms of elementary harmonic functions and complete elliptical integrals. For an ease of reference, the formulations of the fundamental solutions are briefly outlined in the following.

Case a: $\Delta_1 \ne 0$ and $\Delta_2 \ne 0$

(i) In the solid $k = 1(z \ge 0)$, we have

$$\begin{aligned}\mathbf{u} = \Big\{ & \mathbf{G}_v\left[0, z_{01}, \boldsymbol{\Phi}_{01}\right] + \sum_{n=1}^{4} \mathbf{G}_v\left[0, z_{n1}, \boldsymbol{\Phi}_{an1}\right] + \mathbf{G}_v\left[0, \gamma_{01}|\underline{z}|, \boldsymbol{\Phi}_v\right] \\ & + \mathbf{G}_v\left[0, \gamma_{11}|\underline{z}|, \boldsymbol{\Phi}_u\left(\gamma_{11}\right)\right] - \mathbf{G}_v\left[0, \gamma_{21}|\underline{z}|, \boldsymbol{\Phi}_u\left(\gamma_{21}\right)\right]\Big\}\mathbf{F}\end{aligned}$$

$$\begin{aligned}\mathbf{T}_Z = \Big\{ & \mathbf{G}_v\left[1, z_{01}, \boldsymbol{\Psi}_{01}\right] + \sum_{n=1}^{4} \mathbf{G}_v\left[1, z_{n1}, \boldsymbol{\Psi}_{an1}\right] \\ & + \mathbf{G}_v\left[1, \gamma_{01}|\underline{z}|, \boldsymbol{\Psi}_v\right] + \mathbf{G}_v\left[1, \gamma_{11}|\underline{z}|, \boldsymbol{\Psi}_u\left(\gamma_{11}\right)\right] \\ & - \mathbf{G}_v\left[1, \gamma_{21}|\underline{z}|, \boldsymbol{\Psi}_u\left(\gamma_{21}\right)\right]\Big\}\mathbf{F}\end{aligned} \tag{A4}$$

$$\begin{aligned}\mathbf{\Gamma}_p = \Big\{&\mathbf{G}_p\Big[1, z_{01}, \mathbf{\Phi}_{01}\Big] + \sum_{n=1}^{4} \mathbf{G}_p\Big[1, z_{n1}, \mathbf{\Phi}_{an1}\Big] \\ &+ \mathbf{G}_p\Big[1, \gamma_{01}|\underline{z}|, \mathbf{\Phi}_v\Big] \\ &+ \mathbf{G}_p\Big[1, \gamma_{11}|\underline{z}|, \mathbf{\Phi}_u\Big(\gamma_{11}\Big)\Big] \\ &- \mathbf{G}_p\Big[1, \gamma_{21}|\underline{z}|, \mathbf{\Phi}_u\Big(\gamma_{21}\Big)\Big]\Big\}\mathbf{F}\end{aligned}$$

(ii) In the solid $k = 2(z \le 0)$, we have

$$\begin{aligned}\mathbf{u} &= \left\{\mathbf{G}_v[0, z_{02}, \mathbf{\Phi}_{02}] + \sum_{n=1}^{4} \mathbf{G}_v[0, z_{n2}, \mathbf{\Phi}_{an2}]\right\}\mathbf{F} \\ \mathbf{T}_z &= \left\{\mathbf{G}_v[1, z_{02}, \mathbf{\Psi}_{02}] + \sum_{n=1}^{4} \mathbf{G}_v[1, z_{n2}, \mathbf{\Psi}_{an2}]\right\}\mathbf{F} \\ \mathbf{\Gamma}_p &= \left\{\mathbf{G}_p[1, z_{02}, \mathbf{\Phi}_{02}] + \sum_{n=1}^{4} \mathbf{G}_p[1, z_{n2}, \mathbf{\Phi}_{an2}]\right\}\mathbf{F}\end{aligned} \tag{A5}$$

where $z_{01} = \gamma_{01}(z + h)$, $z_{11} = \gamma_{11}(z + h)$, $z_{21} = \gamma_{21}z + \gamma_{11}h$, $z_{31} = \gamma_{11}z + \gamma_{21}h$, $z_{41} = \gamma_{21}(z + h)$, $z_{02} = \gamma_{01}h - \gamma_{02}z$, $z_{12} = \gamma_{11}h - \gamma_{12}z$, $z_{22} = \gamma_{11}h - \gamma_{22}z$, $z_{32} = \gamma_{21}h - \gamma_{12}z$, $z_{42} = \gamma_{21}h - \gamma_{22}z$. γ_{0k}, γ_{1k} and γ_{2k} $(k = 1, 2)$ are given as follows,

$$\gamma_{0k} = \sqrt{c_{5k}/c_{4k}},$$

$$\begin{aligned}\gamma_{1k} = \frac{1}{2\sqrt{c_{3k}c_{4k}}}\Big[&\sqrt{(\sqrt{c_{1k}c_{3k}} - c_{2k})(\sqrt{c_{1k}c_{3k}} + c_{2k} + 2c_{4k})} \\ &+ \sqrt{(\sqrt{c_{1k}c_{3k}} + c_{2k})\Delta_k}\Big],\end{aligned}$$

$$\begin{aligned}\gamma_{2k} = \frac{1}{2\sqrt{c_{3k}c_{4k}}}\Big[&\sqrt{(\sqrt{c_{1k}c_{3k}} - c_{2k})(\sqrt{c_{1k}c_{3k}} + c_{2k} + 2c_{4k})} \\ &- \sqrt{(\sqrt{c_{1k}c_{3k}} + c_{2k})\Delta_k}\Big].\end{aligned}$$

Case b: $\Delta_1 = 0$ and $\Delta_2 \neq 0$

(i) In the solid $k = 1(z \ge 0)$, we have

$$\begin{aligned}\mathbf{u} = \Big\{&\mathbf{G}_v\Big[0, z_{01}, \mathbf{\Phi}_{01}\Big] + \mathbf{G}_v\Big[0, z_{a0}, \mathbf{\Phi}_{b11}\Big] \\ &+ z\mathbf{G}_v\Big[1, z_{a0}, \mathbf{\Phi}_{b21}\Big] + h\mathbf{G}_v\Big[1, z_{a0}, \mathbf{\Phi}_{b31}\Big] \\ &+ zh\mathbf{G}_v\Big[2, z_{a0}, \mathbf{\Phi}_{b41}\Big] + \mathbf{G}_v\Big[0, \gamma_{01}|\underline{z}|, \mathbf{\Phi}_v\Big] \\ &+ \mathbf{G}_v\Big[0, \gamma_a|\underline{z}|, \mathbf{\Phi}_x\Big] + \underline{z}\mathbf{G}_v\Big[1, \gamma_a|\underline{z}|, \mathbf{\Phi}_y\Big]\Big\}\mathbf{F}\end{aligned}$$

$$\begin{aligned}\mathbf{T} = \Big\{&\mathbf{G}_v\Big[1, z_{01}, \mathbf{\Psi}_{01}\Big] + \mathbf{G}_v\Big[1, z_{a0}, \mathbf{\Psi}_{b11}\Big] \\ &+ z\mathbf{G}_v\Big[2, z_{a0}, \mathbf{\Psi}_{b21}\Big] + h\mathbf{G}_v\Big[2, z_{a0}, \mathbf{\Psi}_{b31}\Big] \\ &+ zh\mathbf{G}_v\Big[3, z_{a0}, \mathbf{\Psi}_{b41}\Big] + \mathbf{G}_v\Big[1, \gamma_{01}|\underline{z}|, \mathbf{\Psi}_v\Big] \\ &+ \mathbf{G}_v\Big[1, \gamma_a|\underline{z}|, \mathbf{\Psi}_x\Big] + \underline{z}\mathbf{G}_v\Big[2, \gamma_a|\underline{z}|, \mathbf{\Psi}_y\Big]\Big\}\mathbf{F}\end{aligned} \tag{A6}$$

$$\begin{aligned}\mathbf{\Gamma}_p = \Big\{&\mathbf{G}_p\Big[1, z_{01}, \mathbf{\Phi}_{01}\Big] + \mathbf{G}_p\Big[1, z_{a0}, \mathbf{\Phi}_{b11}\Big] \\ &+ z\mathbf{G}_p\Big[2, z_{a0}, \mathbf{\Phi}_{b21}\Big] + h\mathbf{G}_p\Big[2, z_{a0}, \mathbf{\Phi}_{b31}\Big] \\ &+ zh\mathbf{G}_p\Big[3, z_{a0}, \mathbf{\Phi}_{b41}\Big] + \mathbf{G}_p\Big[1, \gamma_{01}|\underline{z}|, \mathbf{\Phi}_v\Big] \\ &+ \mathbf{G}_p\Big[1, \gamma_a|\underline{z}|, \mathbf{\Phi}_x\Big] + \underline{z}\mathbf{G}_p\Big[2, \gamma_a|\underline{z}|, \mathbf{\Phi}_y\Big]\Big\}\mathbf{F}\end{aligned}$$

(ii) In the solid $k = 2(z \le 0)$, we have

$$\begin{aligned}\mathbf{u} = \Big\{&\mathbf{G}_v\Big[0, z_{02}, \mathbf{\Phi}_{02}\Big] + \mathbf{G}_v\Big[0, z_{a1}, \mathbf{\Phi}_{b12}\Big] \\ &+ h\mathbf{G}_v\Big[1, z_{a1}, \mathbf{\Phi}_{b22}\Big] + \mathbf{G}_v\Big[0, z_{a2}, \mathbf{\Phi}_{b32}\Big] \\ &+ h\mathbf{G}_v\Big[1, z_{a2}, \mathbf{\Phi}_{b42}\Big]\Big\}\mathbf{F}\end{aligned}$$

$$\begin{aligned}\mathbf{T}_z = \Big\{&\mathbf{G}_v\Big[1, z_{02}, \mathbf{\Psi}_{02}\Big] + \mathbf{G}_v\Big[1, z_{a1}, \mathbf{\Psi}_{b12}\Big] \\ &+ h\mathbf{G}_v\Big[2, z_{a1}, \mathbf{\Psi}_{b22}\Big] + \mathbf{G}_v\Big[1, z_{a2}, \mathbf{\Psi}_{b32}\Big] \\ &+ h\mathbf{G}_v\Big[2, z_{a2}, \mathbf{\Psi}_{b42}\Big]\Big\}\mathbf{F}\end{aligned} \tag{A7}$$

$$\begin{aligned}\mathbf{\Gamma}_p = \Big\{&\mathbf{G}_p\Big[1, z_{02}, \mathbf{\Phi}_{02}\Big] + \mathbf{G}_p\Big[1, z_{a1}, \mathbf{\Phi}_{b12}\Big] \\ &+ h\mathbf{G}_p\Big[2, z_{a1}, \mathbf{\Phi}_{b22}\Big] + \mathbf{G}_p\Big[1, z_{a2}, \mathbf{\Phi}_{b32}\Big] \\ &+ h\mathbf{G}_p\Big[2, z_{a2}, \mathbf{\Phi}_{b42}\Big]\Big\}\mathbf{F}\end{aligned}$$

where $z_{a0} = \gamma_a(z + h)$, $z_{a1} = \gamma_a h - \gamma_{12}z$, $z_{a2} = \gamma_a h - \gamma_{22}z$, $\gamma_{11} = \gamma_{21} = \gamma_a$ and $\gamma_{12} = \gamma_{22} = \gamma_b$.

Case c: $\Delta_1 \neq 0$ and $\Delta_2 = 0$

In this case, the solutions for $\mathbf{u}, \mathbf{T}_z$ and $\mathbf{\Gamma}_p$ in the solid $k = 1(z \ge 0)$ can be obtained by substituting γ_b for γ_{22} in Eqs. (A4) for case a. in the solid $k = 2(z \le 0)$, we have

$$\begin{aligned}\mathbf{u} = \Big\{&\mathbf{G}_v\Big[0, z_{02}, \mathbf{\Phi}_{02}\Big] + \mathbf{G}_v\Big[0, z_{b1}, \mathbf{\Phi}_{c12}\Big] \\ &+ z\mathbf{G}_v\Big[1, z_{b1}, \mathbf{\Phi}_{c22}\Big] + \mathbf{G}_v\Big[0, z_{b2}, \mathbf{\Phi}_{c32}\Big] \\ &+ z\mathbf{G}_v\Big[1, z_{b2}, \mathbf{\Phi}_{c42}\Big]\Big\}\mathbf{F}\end{aligned}$$

$$\begin{aligned}\mathbf{T}_z = \Big\{&\mathbf{G}_v\Big[1, z_{02}, \mathbf{\Psi}_{02}\Big] + \mathbf{G}_v\Big[1, z_{b1}, \mathbf{\Psi}_{c12}\Big] \\ &+ z\mathbf{G}_v\Big[2, z_{b1}, \mathbf{\Psi}_{c22}\Big] + \mathbf{G}_v\Big[1, z_{b2}, \mathbf{\Psi}_{c32}\Big] \\ &+ z\mathbf{G}_v\Big[2, z_{b2}, \mathbf{\Psi}_{c42}\Big]\Big\}\mathbf{F}\end{aligned} \tag{A8}$$

$$\begin{aligned}\mathbf{\Gamma}_p = \Big\{&\mathbf{G}_p\Big[1, z_{02}, \mathbf{\Phi}_{02}\Big] + \mathbf{G}_p\Big[1, z_{b1}, \mathbf{\Phi}_{c12}\Big] \\ &+ z\mathbf{G}_p\Big[2, z_{b1}, \mathbf{\Phi}_{c22}\Big] + \mathbf{G}_p\Big[1, z_{b2}, \mathbf{\Phi}_{c32}\Big] \\ &+ h\mathbf{G}_p\Big[2, z_{b2}, \mathbf{\Phi}_{c42}\Big]\Big\}\mathbf{F}\end{aligned}$$

where $z_{b1} = \gamma_{11}h - \gamma_b z$ and $z_{b2} = \gamma_{21}h - \gamma_b z$

Case d: $\Delta_1 = 0$ and $\Delta_2 = 0$

In this case, the solutions for $\mathbf{u}, \mathbf{T}_z$ and $\mathbf{\Gamma}_p$ in the solid $k = 1(z \ge 0)$ can be obtained by substituting γ_b for γ_{12}

and γ_{22} in Eqs. (A6) for case b. in the solid $k = 2(z \le 0)$, we have

$$\begin{aligned}\mathbf{u} &= \Big\{\mathbf{G}_v\Big[0, z_{02}, \mathbf{\Phi}_{02}\Big] + \mathbf{G}_v\Big[0, z_{ab}, \mathbf{\Phi}_{d12}\Big] \\ &\quad + z\mathbf{G}_v\Big[1, z_{ab}, \mathbf{\Phi}_{d22}\Big] + h\mathbf{G}_v\Big[1, z_{ab}, \mathbf{\Phi}_{d32}\Big] \\ &\quad + zh\mathbf{G}_v\Big[2, z_{ab}, \mathbf{\Phi}_{d42}\Big]\Big\}\mathbf{F} \\ \mathbf{T}_z &= \Big\{\mathbf{G}_v\Big[1, z_{02}, \mathbf{\Psi}_{02}\Big] + \mathbf{G}_v\Big[1, z_{ab}, \mathbf{\Psi}_{d12}\Big] \\ &\quad + z\mathbf{G}_v\Big[2, z_{ab}, \mathbf{\Psi}_{d22}\Big] + h\mathbf{G}_v\Big[2, z_{ab}, \mathbf{\Psi}_{d32}\Big] \\ &\quad + zh\mathbf{G}_v\Big[3, z_{ab}, \mathbf{\Psi}_{d42}\Big]\Big\}\mathbf{F} \qquad \text{(A9)} \\ \mathbf{\Gamma}_p &= \Big\{\mathbf{G}_p\Big[1, z_{02}, \mathbf{\Phi}_{02}\Big] + \mathbf{G}_p\Big[1, z_{ab}, \mathbf{\Phi}_{d12}\Big] \\ &\quad + z\mathbf{G}_p\Big[2, z_{ab}, \mathbf{\Phi}_{d22}\Big] + h\mathbf{G}_p\Big[2, z_{ab}, \mathbf{\Phi}_{d32}\Big] \\ &\quad + zh\mathbf{G}_p\Big[3, z_{ab}, \mathbf{\Phi}_{d42}\Big]\Big\}\mathbf{F}\end{aligned}$$

where $z_{ab} = \gamma_a h - \gamma_b z$.

In the above equations, the fundamental solution matrices $\mathbf{G}_v[n, z, \mathbf{\Phi}]$ and $\mathbf{G}_p[n, z, \mathbf{\Phi}]$ $(n = 0, 1, 2, 3;\ z \ge 0)$ are defined in the following,

$$\begin{aligned}4\pi\mathbf{G}_v[n, z, \mathbf{\Phi}] &= \phi_{22}\begin{pmatrix} g_{n02}(z) & -g_{n11}(z) & 0 \\ -g_{n11}(z) & g_{n20}(z) & 0 \\ 0 & 0 & 0 \end{pmatrix} \\ &\quad + \begin{pmatrix} \phi_{11}g_{n20}(z) & \phi_{11}g_{n11}(z) & \phi_{13}g_{n10}(z) \\ \phi_{11}g_{n11}(z) & \phi_{11}g_{n02}(z) & \phi_{13}g_{n01}(z) \\ -\phi_{31}g_{n10}(z) & -\phi_{31}g_{n01}(z) & \phi_{33}g_{n00}(z) \end{pmatrix} \\ &4\pi\mathbf{G}_p[n, z, \mathbf{\Phi}] \\ &= \phi_{22}\begin{pmatrix} g_{n12}(z) & -g_{n21}(z) & 0 \\ \frac{1}{2}[g_{n03}(z) - g_{n21}(z)] & \frac{1}{2}[g_{n30}(z) - g_{n12}(z)] & 0 \\ -g_{n12}(z) & g_{n21}(z) & 0 \end{pmatrix} \\ &\quad + \begin{pmatrix} \phi_{11}g_{n30}(z) & \phi_{11}g_{n21}(z) & -\phi_{13}g_{n20}(z) \\ \phi_{11}g_{n21}(z) & \phi_{11}g_{n12}(z) & -\phi_{13}g_{n11}(z) \\ \phi_{11}g_{n12}(z) & \phi_{11}g_{n03}(z) & -\phi_{13}g_{n02}(z) \end{pmatrix}\end{aligned} \qquad \text{(A10)}$$

where $z > 0$; $n = 0, 1, 2, 3$, and the harmonic functions $g_{0lm}(z)$ are given by

$$\begin{aligned} g_{000}(z) &= \frac{1}{R}, \\ g_{002}(z) &= \frac{1}{R_z}\left[1 - \frac{y^2}{RR_z}\right], \\ g_{010}(z) &= -\frac{x}{RR_z}, \\ g_{030}(z) &= \frac{x}{2R_z^2}\left[\frac{2x^2}{RR_z} - 3\right] \\ g_{001}(z) &= -\frac{y}{RR_z}, \\ g_{011}(z) &= -\frac{xy}{RR_z^2}, \\ g_{021}(z) &= \frac{y}{2R_z^2}\left[\frac{2x^2}{RR_z} - 1\right], \\ g_{020}(z) &= \frac{1}{R_z}\left[1 - \frac{x^2}{RR_z}\right] \\ g_{012}(z) &= \frac{x}{2R_z^2}\left[\frac{2y^2}{RR_z} - 1\right], \\ g_{003}(z) &= \frac{y}{2R_z^2}\left[\frac{2y^2}{RR_z} - 3\right] \end{aligned}$$

where $R = \sqrt{x^2 + y^2 + z^2}$, $R_z = R + z$.

For $n \ge 1$, the harmonic function $g_{nlm}(z)$ $(0 \le l + m \le 3)$ can be obtained by using the following transfer formula,

$$g_{nlm}(z) = -\frac{\partial g_{(n-1)lm}(z)}{\partial z} \qquad \text{(A12)}$$

In equation (A10), the constant matrix $\mathbf{\Phi}$ are defined by

$$\mathbf{\Phi} = \begin{pmatrix} \phi_{11} & 0 & \phi_{13} \\ 0 & \phi_{22} & 0 \\ \phi_{31} & 0 & \phi_{33} \end{pmatrix} \qquad \text{(A13)}$$

Each element of the constant matrix $\mathbf{\Phi}$ depends only on the 10 elastic constants c_{jk} $(j = 1, 2, 3, 4, 5; k = 1, 2)$. Their specific forms can be found in Yue (1995).

Acknowledgements The work presented in this paper was supported by the Research Grants Council of Hong Kong SAR Government. The authors would like to thank the Editor-In-Chief Prof. P. Wriggers, the Associate Editor Prof. D. E. Beskos and the two peer reviewers for their valuable comments and suggestions, which enhanced the presentation of the paper.

References

Aliabadi MH (1997) Boundary element formulations in fracture mechanics. ASME Appl Mech Rev 1997, 50:83–96

Ariza MP, Dominguez J (2004) Boundary element formulation for 3D transversely isotropic cracked bodies. Int J Numer Meth Eng 60:719–753

Kassir MK, Sih GC (1968) Three-dimensional stresses around elliptical cracks in transversely isotropic solids. Eng Fract Mech 1:327–345

Kassir MK, Sih GC (1975) Three-dimensional crack problems. Noordhoff International Publishing, pp. 336–381

Sih GC, Chen EP (1981) Cracks in composites. Martinus Nijhoff Publishers

Lin W, Keer LM (1989) Three-dimensional analysis of cracks in layered transversely isotropic media. Proceedings of Royal Society (London) A424:307–322

Jia ZH, Shippy DJ, Rizzo FJ (1989) Three-dimensional crack analysis using singular boundary elements. Int J Numer Meth Eng 28:2257–2273

Kou CH, Keer LM (1995) Three-dimensional analysis of cracking in a multilayered composite. ASME J Appl Mech 62:273–281

Kassir MK, Sih GC (1966) Three-dimensional stress distribution around an elliptical crack under arbitrary loadings. ASME J Appl Mech. 33:601–611

Luchi ML, Rizzuti S (1987) Boundary elements of for three-dimensional elastic crack analysis. Int J Numer Meth Eng 24:2253–2271

Mura T (1982) Micromechanics of defects in solids. The Hague: Martinus Nijhoff

Hoeing A (1978) The behavior of a flat elliptical crack in an anisotropic elastic body. Int J Solids Struct 14:925–934

Ozturk M, Erdogan F (1996) Axisymmetric crack problem in bonded materials with a nonhomogenous interfacial region. Int J Solids Struct 33:4101–4117

Pan E, Amadei B (1999) Boundary element analysis of fracture mechanics in anisotropic bimaterials. Eng Anal Bound Elem 23:683–691

Pan E, Yuan FG (2000) Boundary element analysis of three-dimensional cracks in anisotropic solids. Int J Numer Meth Eng 48:211–237

Pan YC, Chou TW (1976) Point force solution for an infinite transversely isotropic solid. ASME J Appl Mech 43:608–612

Saez A, Ariza, Dominguez J (1997) Three-dimensional fracture analysis in transversely isotropic solids. Eng Anal Bound Elem 20:287–298

Sih GC, Paris PC, Irwin GR (1965) On crack in rectilinearly anisotropic bodies. Int J Fract 1:189–203

Suo Z (1990) Singularities, interfaces and cracks in dissimilar anisotropic media. Proceedings of Royal Society (London) A427:331–358

Sollero P, Aliabadi MH (1993) Fracture mechanics analysis of anisotropic composite laminates by the boundary element method. Int J Frac 64:269–284

Sollero P, Aliabadi MH (1995) Anisotropic analysis of cracks in composite laminates using the dual boundary element method. Composite Struct 31:229–234

Tan CL, Gao YL (1992) Boundary integral equation fracture mechanics analysis of plane orthotropic bodies. Int J Frac 53:343–365

Ting TCT (1996) Anisotropic elasticity: theory and applications. New York: Oxford University Press

Xiao HT, Yue ZQ, Tham LG, Chen YR (2005) Stress intensity factors for penny-shaped cracks perpendicular to graded interfacial zone of bonded bi-materials. Eng Frac Mech. 72:121–143

Yang B (2002) Examination of free-edge crack nucleation around an open hole in composite laminates. Int J Frac 115:173–191

Yue ZQ (1995) Elastic fields in two joined transversely isotropic solids due to concentrated forces. Int J Eng Sci 33:351–369

Yue ZQ, Xiao HT (2002) Generalized Kelvin solution based boundary element method for crack problems in multilayered solids. Eng Anal Bound Elem 26: 691–705

Yue ZQ, Xiao HT, Tham LG (2003) Boundary element analysis of crack problems in functionally graded materials. Int J Solids Struct 40:3273–3291

Zhang ZG, Mai YW (1989) A simple solution for the stress intensity factor of a flat elliptical crack in a transversely isotropic solid. Eng Frac Mech 34:645–648